Quantum Electronics **48** (2) 129–135 (2018)

https://doi.org/10.1070/QEL16522

Generation of light and dark soliton trains in a dissipative four-wave mixing, mode-locked fibre ring laser

I.O. Zolotovskii, D.A. Korobko, A.A. Sysolyatin

Abstract. **We consider a model of a dissipative four-wave mixing, mode-locked fibre ring laser with an intracavity interferometer. The necessary conditions required for mode locking are presented. A pulse train generation is numerically simulated at different repetition rates and gain levels. Admissible ranges of values, for which successful mode locking is possible, are found. It is shown that in the case of normal dispersion of the resonator, a laser with an intracavity interferometer can generate a train of pulses with an energy much greater than that in the case of anomalous dispersion.**

Keywords: *generation of high-repetition-rate pulse trains, fibre ring laser, dissipative four-wave mixing.*

1. Introduction

Laser sources of high-repetition-rate ultrashort pulses are in demand in a number of applications of modern photonics, i.e. optical communication, signal processing, comb spectrum generation, etc. [1–3]. One of popular variants of such sources are short-cavity lasers, for example, semiconductor disk lasers, which make it possible to achieve a repetition rate of hundreds of GHz [4, 5]. One more variant combining the advantages, such as compactness, reliability, high beam quality, convenient output, etc., is passive harmonically mode-locked soliton fibre lasers [6, 7]. The most common mechanism of mode locking in fibre lasers is the use of saturable absorbers or schemes with a nonlinear dependence of transmission on power, in particular, due to nonlinear polarisation evolution (NPE) [8, 9]. In these schemes, a uniform distribution of a large number of pulses along the resonator, i.e., harmonic mode locking, results from mutual repulsion of pulses, for example, due to gain saturation and relaxation [10, 11]. However, it is shown that this mechanism is not stable at sufficiently close interpulse distances, i.e., at high repetition rates [12–14].

A so-called self-induced modulation instability based on dissipative four-wave mixing (DFWM) is a promising mechanism for realising harmonic mode locking with a high repetition rate in fibre lasers [15, 16]. The essence of this effect is that among a set of longitudinal resonator modes it is necessary to select only two (symmetric with respect to the gain maximum) modes, in which the gain exceeds the losses. The remaining modes generated during the four-wave mixing (FWM) process are located in the frequency domain where the losses predominate, and they receive energy only through parametric interaction.

The key element of such a scheme is a high-Q filter, which allows selection of the above two main modes and suppression of all other modes of the resonator in the region of positive gain, i.e., in the frequency range where the gain exceeds the losses. A similar filter can be, for example, a Fabry–Perot interferometer. Also promising is the use of a high-Q fibre-coupled microcavity, with the latter being not only a filter, but also a nonlinear element [17].

As a result of filtration, a comb-like equidistant spectrum is formed in the resonator. Then, in the course of nonlinear FWM, all its harmonics, i.e. cavity modes remaining after filtering, are automatically locked [18, 19]. In the time representation, this pattern is equivalent to generation of pulses uniformly distributed over the resonator, with a repetition rate equal to the frequency difference of the original fundamental central modes. The repetition rate is given by the free spectral parameter (FSR) of the filter, and its maximum (in the ideal case of a filter with an infinitely high resolution) is limited only by the width of the gain line. The use of such a scheme allows the generation of pulse trains with a repetition rate of up to 1 THz and higher [17, 20].

Korobko et al. [21] considered a model of a fibre ring laser with an intracavity interferometer, which generates a regular pulse train with a widely tunable repetition rate (with a change in the FSR of the interferometer). One of the results of work [21] is the establishment of the fact that mode locking via DFWM can be realised in a wide range of repetition rates, while an important role is played by the tuning of polarisers, which eliminates the mode locking through nonlinear polarisation evolution. Harmonic NPE mode locking can also be realised in this scheme, but only in a rather narrow range and at much lower repetition rates. One of the variants of NPE mode locking is the formation of pulse structures that are different from a train of pulses uniformly distributed across the cavity, for example, pulse trains with an interpulse distance controlled by means of an interferometer [22]. The obtained results are in qualitative agreement with the experimental data [20, 22, 23].

In the present work, we continue to study the features of DFWM mode locking in a fibre ring laser with a built-in

I.O. Zolotovskii, D.A. Korobko Ulyanovsk State University, ul. L. Tolstogo 42, 432700 Ulyanovsk, Russia; e-mail: korobkotam@rambler.ru;
A.A. Sysolyatin A.M. Prokhorov General Physics Institute, Russian Academy of Sciences, ul. Vavilova 38, 119991 Moscow, Russia; Ulyanovsk State University, ul. L. Tolstogo 42, 432700 Ulyanovsk, Russia

Received 26 September 2017; revision received 27 December 2017
Kvantovaya Elektronika **48** (2) 129–135 (2018)
Translated by I.A. Ulitkin

interferometer. The main attention is paid to the selection of modes necessary for generation and to the comparison of the results obtained for anomalous and normal dispersions of the resonator.

2. Model

A typical experimental realisation of the model in question is shown in Fig. 1a. Elements of a fibre ring resonator are an active erbium-doped fibre (EDF), a passive single-mode fibre (SMF) segment, a polarisation-sensitive isolator (PSI) and polarisation controllers (PC1 and PC2). The generated radiation is coupled out from the resonator via a fibre output coupler (OC2). As a built-in intracavity interferometer, we use a tunable Mach–Zehnder interferometer (MZI) with an adjustable optical delay line. The repetition rate of the generated pulse train is determined by the free spectral parameter of the interferometer:

$$\nu \equiv \mathrm{FSR} \tag{1}$$

(for the MZI, FSR = $c/n\Delta L$, where ΔL is the difference between the arms of the interferometer, c is the speed of light, and n is the refractive index of the fibre).

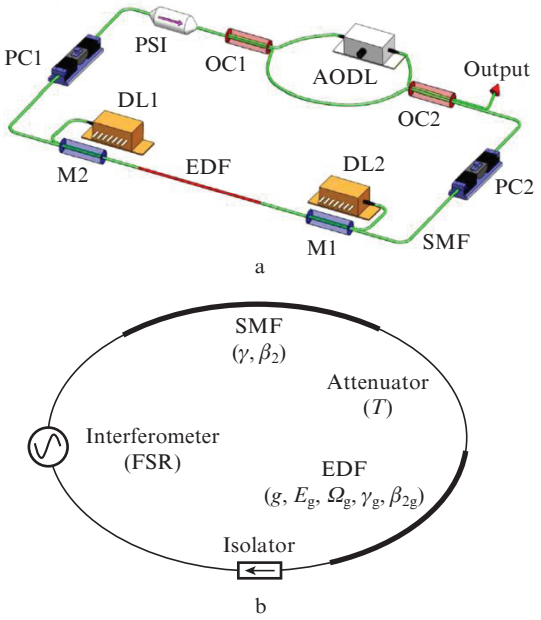

Figure 1. (a) Experimental scheme of a dissipative four-wave mixing, mode-locked laser [20] and (b) resonator scheme used for simulations: (DL1, DL2) pump diode lasers; (M1, M2) multiplexers; (OC1, OC2) output couplers; (PSI) polarisation-sensitive isolator; (AODL) adjustable optical delay line.

Because the purpose of this work is to study mode locking via DFWM, we assume that the polarisation controllers are adjusted so that the light propagation is described by the scalar Ginzburg–Landau equation for one linear polarisation component. This can be done at a certain orientation of the controllers relative to the polarisation vector, with the mode locking being excluded due to the nonlinear polarisation evolution, because the radiation losses during the passage through polarisation-sensitive elements in this case do not depend on the intensity [21]. The equivalent scheme of the resonator, used for simulations, is shown in Fig. 1b.

In simulations we used a classical approach, i.e. the description of the propagation of light in an active fibre using the Ginzburg–Landau equation [24]

$$\frac{\partial A}{\partial z} + \mathrm{i}\frac{\beta_{2\mathrm{g}}}{2}\frac{\partial^2 A}{\partial t^2} - \mathrm{i}\gamma_{\mathrm{g}}|A|^2 A = \frac{gA}{2} + \frac{\beta_{2\mathrm{f}}}{2}\frac{\partial^2 A}{\partial t^2}, \tag{2}$$

where A is the amplitude of the linearly polarised electric field in the fibre; z is the coordinate along the fibre; and $\beta_{2\mathrm{g}}$ and γ_{g} are the group velocity dispersion and Kerr nonlinearity coefficient of the active fibre, respectively. The gain filtering is taken into account in the parabolic approximation: $\beta_{2\mathrm{f}} = g/\Omega_{\mathrm{g}}^2$, where Ω_{g} is the gain line width. The saturated gain factor g is averaged over the simulation window and is expressed as

$$g(z,t) = g(z) = g_0\left(1 + \frac{1}{E_{\mathrm{g}}}\int_0^{\tau_{\mathrm{win}}} |A(z,t)|^2 \mathrm{d}t\right)^{-1}, \tag{3}$$

where g_0 is the small-signal gain; E is the saturation energy of the gain; and τ_{win} is the size of the simulation window. The propagation in a passive SMF is described by the standard nonlinear Schrödinger equation (NSE)

$$\frac{\partial A}{\partial z} - \mathrm{i}\frac{\beta_2}{2}\frac{\partial^2 A}{\partial t^2} - \mathrm{i}\gamma|A|^2 = 0, \tag{4}$$

where β_2 is the group velocity dispersion and γ is the Kerr nonlinearity of the SMF.

The intracavity interferometer is described by the concentrated transfer function $T_{\mathrm{I}} \equiv A'(\Omega)/A(\Omega)$, where $A'(\Omega)$ and $A(\Omega)$ are the input and output amplitudes in the frequency domain. In the model, as a intracavity interferometer, we used a two-pass MZI [25] with a transfer function $T_{\mathrm{I}}(\Omega) \equiv T^2(\Omega)$, where

$$T = R_{\mathrm{MZ}} - (1 - R_{\mathrm{MZ}})\exp(-\mathrm{i}\Omega/\mathrm{FSR}), \tag{5}$$

with the branching ratio of the R_{MZ} signal being assumed close to ideal: $R_{\mathrm{MZ}} = 0.51$. The FSR parameter is chosen so that its transmission maxima $|T_{\mathrm{I}}|$ exactly coincide with the cavity modes. A prerequisite for harmonic mode locking through DFWM is also the fact that the centre gain frequency ω_0 is halfway between the transmission peaks $|T_{\mathrm{I}}|$ of the interferometer. The frequency ω is defined as $\omega = \Omega - \omega_0$. In this case, the resonator modes with frequencies $\omega_{\mathrm{k}} = \pm 2\pi\mathrm{FSR}(1/2 + k)$, where $k = 0, 1, 2, \ldots$, are in the transmission peaks of the interferometer. The frequency difference of the two centre modes $\omega_{\pm 1} = \pm\pi\mathrm{FSR}$ determines the period of the generated pulse train ($t_{\mathrm{rep}} = 1/\mathrm{FSR} = n\Delta L/c$) and specifies the phase difference between adjacent pulses, equal to $\pm\pi$. The latter ensures mutual repulsion of neighbouring pulses and stability of the pulse train, which is extremely important at high pulse repetition rates and small interpulse distances.

Total losses in the resonator (including on connectors and couplers) are taken into account by a separate concentrated transfer function of the attenuator, $T_{\mathrm{att}} \equiv A'(\Omega)/A(\Omega) = \mathrm{const} < 1$, where $A'(\Omega)$ and $A(\Omega)$ are the input and output

Table 1. Parameter values used in simulations.

EDF length /m	SMF length /m	Dispersion $\beta_2 = \beta_{2g}$ /ps^2 km^{-1}	Nonlinearity $\gamma = \gamma_g$ /W^{-1}km^{-1}	Gain g_0 /m^{-1}	Line width Ω_g/ps^{-1}	Transmission coefficient $\lvert T_{att}\rvert^2$ (%)
2.5	5	±2	3.3	3	10	90

amplitude, respectively. Equations (2) and (4) with boundary conditions corresponding to Fig. 1b are modelled using the standard method of stepwise Fourier transforms [24]. The parameters used in the simulation are presented in Table 1. Note that to simplify the discussion we did not consider the dispersion and nonlinear control problem, i.e., the distribution of dispersion and nonlinearity over fibre elements of the resonator is uniform: $\beta_2 = \beta_{2g}, \gamma = \gamma_g$, which corresponds to the total dispersion $B_{2\Sigma} = \pm 0.015$ ps^2 and the nonlinearity $\Gamma_\Sigma = 0.025$ W^{-1}. Different signs of the dispersion $B_{2\Sigma}$ indicate that cases of both anomalous and normal dispersion of the resonator were considered.

The gain line in the parabolic approximation is defined as $g(z)(1 - \omega^2/\Omega_g^2)$ with the full width at half maximum $\Delta\omega = \sqrt{2}\Omega_g$. Thus, for $\lambda = 1.55$ μm, the chosen width $\Delta\lambda$ corresponds to ~18 nm, which agrees with the parameters of modern amplifying structures based on erbium-doped fibres. The saturation energy, determined by the pump power, varied in the range from 0.5 to 50 pJ in the simulation window $\tau_{win} = 2^{12} \times 0.0125$ ps = 5.12 ps at different FSR values of the interferometer. A change in the saturation energy made it possible to change in simulation the value of the frequency domain in which the gain exceeded the losses. For example, to generate a train of pulses with a repetition rate of ~1 THz in a resonator with the anomalous total dispersion of $B_{2\Sigma} = -0.015$ ps^2, it is necessary to set $E_g = 0.8$ pJ, which provides the required positive gain bandwidth (slightly more than $2\pi \times 10^{12}$ s^{-1} ≈ 7 nm for the wavelength $\lambda = 1.55$ μm). The purpose of the numerical experiments was to find the region of variation of the parameters in which it is possible to implement mode locking through DFWM.

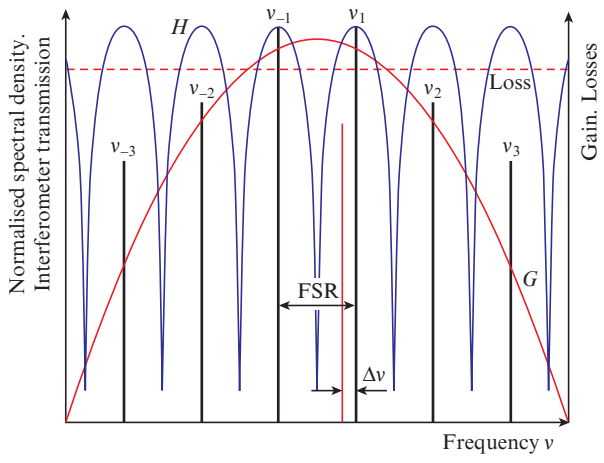

Figure 2. Scheme of the fundamental mode (ν_1 and ν_{-1}) filtration and nonfundamental mode ($\nu_{\pm 2}$ and $\nu_{\pm 3}$) generation during mode locking through dissipative four-wave mixing: G is the gain; H is the transmission of the interferometer; Loss is the level of losses; vertical lines are the amplitudes of modes.

3. Mechanism of mode locking through dissipative four-wave mixing (necessary conditions)

In this section, we consider the main features of the processes occurring in a DFWM fibre laser cavity and introduce the main notations, which are illustrated in Fig. 2. The most important point is the separation of the two main resonator modes ν_1 and ν_{-1}, located symmetrically with respect to the gain maximum G. In the frequency domain in which the value of the total gain G exceeds the total losses of the resonator (they include output losses, fibre attenuation, splicing losses, etc.), only these modes should exist. This frequency domain is called the region of positive gain. As already noted, we assume that the nonlinear losses caused by the passage through polarisation-sensitive elements are eliminated by adjusting the polarisers. Thus, the losses considered are spectrally homogeneous and completely linear, i.e., they do not depend on the radiation power. As a result, the width of the positive gain band, where the condition $G_+(\omega) > 0$ is satisfied,

$$G_+ = G - \text{Loss},$$

$$G = \exp\left[\int g(z,\omega)\,dz\right] = \exp\left\{\int g(z)[1 - (\omega/\Omega_g)^2]dz\right\},$$

is determined only by the parameters of the active fibre – the gain line width Ω_g, small-signal gain g_0 and saturation energy E_g.

The frequency separation between the two main symmetrical modes of the resonator, ν_1 and ν_{-1}, is determined by the FSR parameter of the intracavity interferometer (for example, a constant of the Fabry–Perot interferometer, or a path difference in the MZI). After mode locking, this frequency separation determines the repetition rate of the pulses generated in the resonator. Since the nonfundamental modes of the resonator, ν_k ($|k| > 1$), are formed via FWM of the fundamental modes, all frequencies of the resonator modes can be expressed as $\nu_k = \text{FSR}(k \mp 1/2)$, where the sign '–' is chosen for $k > 0$, and '+' for $k < 0$. It is also important to note that the selectivity of any intracavity interferometer decreases with increasing FSR, i.e., the filtering of side modes at high FSR values becomes more difficult.

The conclusion from the above discussion is that for the necessary modes to be successfully assigned, two main conditions must be fulfilled simultaneously; when they are executed, the DFWM-based mode locking is automatic. First, all resonator modes (except for the fundamental ones, ν_1 and ν_{-1}) must be outside the region of positive gain, i.e.,

$$G_+\left(\pm\frac{3}{2}\text{FSR}\right) < 0. \qquad (6)$$

Secondly, the intracavity interferometer should ensure that all side modes are filtered in the transmission peaks closest to the gain maximum. The frequencies of the neighbouring modes of the laser resonator after filtration differ from each other by the value $\Delta\nu = 1/T_r < \text{FSR}$, where T_r is the round-trip time of the resonator. A prerequisite is that the transmission difference of the interferometer, $H(\nu)$, for the fundamental and side modes should be higher than the difference in the total gain experienced by these modes. Figure 2 shows these differences for the fundamental mode ν_1 and the nearest side mode:

$G_+(\mathrm{FSR}/2 - \Delta\nu) - G_+(\mathrm{FSR}/2) < H(\mathrm{FSR}/2) - H(\mathrm{FSR}/2 - \Delta\nu)$.

Taking into account $\mathrm{d}H/\mathrm{d}\nu = 0$ for $\nu = \mathrm{FSR}/2$, one can obtain

$$\frac{\mathrm{d}G_+}{\mathrm{d}\nu}(\mathrm{FSR}/2) < \frac{1}{2}\frac{\mathrm{d}^2H}{\mathrm{d}\nu^2}(\mathrm{FSR}/2)\Delta\nu. \qquad (7)$$

It can be seen that condition (7) is more easily satisfied for short resonators with a relatively large free spectral range $\Delta\nu$ and a broad gain line. To fulfil this condition, a high selectivity of the intracavity interferometer is also required (the second derivative $\mathrm{d}^2H/\mathrm{d}\nu^2$ should assume a large positive value in the transmission maximum at $\nu = \mathrm{FSR}/2$). Because the selectivity of the interferometer decreases with increasing FSR, and the value of $\mathrm{d}G_+/\mathrm{d}\nu$ increases, then at a certain maximum value of FSR condition (7) ceases to be satisfied, i.e., it limits the maximum achievable repetition rate $\mathrm{FSR}_{\max}$ of pulses obtained via DFWM.

Condition (6), in turn, is satisfied starting from some minimum value $\mathrm{FSR}_{\min}$, i.e., it limits the minimum achievable repetition rate. If the condition $\mathrm{FSR}_{\max} > \mathrm{FSR}_{\min}$ is fulfilled, the system can successfully generate pulse trains via DFWM; in the $\mathrm{FSR}_{\min} - \mathrm{FSR}_{\max}$ range, it is in principle possible to adjust the repetition rate due to local adjustment or the replacement of the intracavity interferometer by an element with a different FSR value.

The width of the pulse spectrum increases with increasing integral gain in the system; therefore, in the indicated band of the generated pulse rates, $\mathrm{FSR}_{\min} - \mathrm{FSR}_{\max}$, for each FSR value there exists an interval of the integral gain $G_{\min} - G_{\max}$, in which conditions (6) and (7) are satisfied. At the extreme points of $\mathrm{FSR}_{\min}$ and $\mathrm{FSR}_{\max}$, this interval closes, and at some intermediate FSR point the interval $G_{\min} - G_{\max}$ is maximal, and so the region of conditions (6) and (7) is bounded on the plane (FSR, G) by the curves connecting the vertex of the maximum gain with the extreme points ($\mathrm{FSR}_{\min}$, $G_{\min 1}$) and ($\mathrm{FSR}_{\max}$, $G_{\min 2}$). From the physical point of view, instead of the integral gain, it is more instructive to use the saturation energy E_g, which characterises the pumping at a given small-signal gain g_0. As a result, the region of successful selection of the main resonator modes (or, in other words, the mode-locking region) can be represented in coordinates (FSR, E_g). Examples of such regions are given in Section 4 (Fig. 5).

The resulting relation (7) also makes it possible to more accurately interpret the results of numerical simulation of the system. Indeed, in numerical calculations, the free spectral range of the resonator is inversely proportional to the size of the simulation window. For the window ~100 ps, $\nu = 10$ GHz. In real fibre systems, the intermode distance ν does not exceed hundreds of MHz. Thus, for the adequacy of the results in the simulation, it is necessary to use an interferometer with a much lower selectivity in comparison with the interferometer used in the real system. The width of the transmission peak of the interferometer (5) used at half-height is approximately 1/6 FSR. A model system with such an interferometer can be compared with a real system including a Fabry–Perot interferometer with a high reflection coefficient R_{FP} of the mirrors. The width of its transmission peak at half-height is $\mathrm{FSR}(1 - R_{FP})/(\pi\sqrt{R_{FP}})$, which at $R_{FP} = 0.9974$ gives a value close to 1/1200 FSR. Thus, from the point of view of the density of filtered modes, the model under consideration with a two-pass MZI is equivalent to a system containing a high-Q Fabry–Perot interferometer with a resonator round-trip time T_r, approximately 200 times larger than the simulation window.

4. Simulation results

This section presents the results of numerical simulation of the system under study, obtained for different FSR values of an intracavity interferometer. In their analysis, attention will be focused mainly on how the dispersion properties of the resonator affect the characteristics of the generated pulses. As the initial conditions, the small amplitude noise, consisting of 1000 modes with Gaussian statistics, is selected. The results show that for selected parameters corresponding to real laser systems, after several thousand round-trips of the resonator, the modes are locked through DFWM and a regular train of pulses with a repetition rate equal to FSR is formed.

First we consider the case of anomalous dispersion of the resonator. Figures 3 and 4 (upper row) show the spectra and

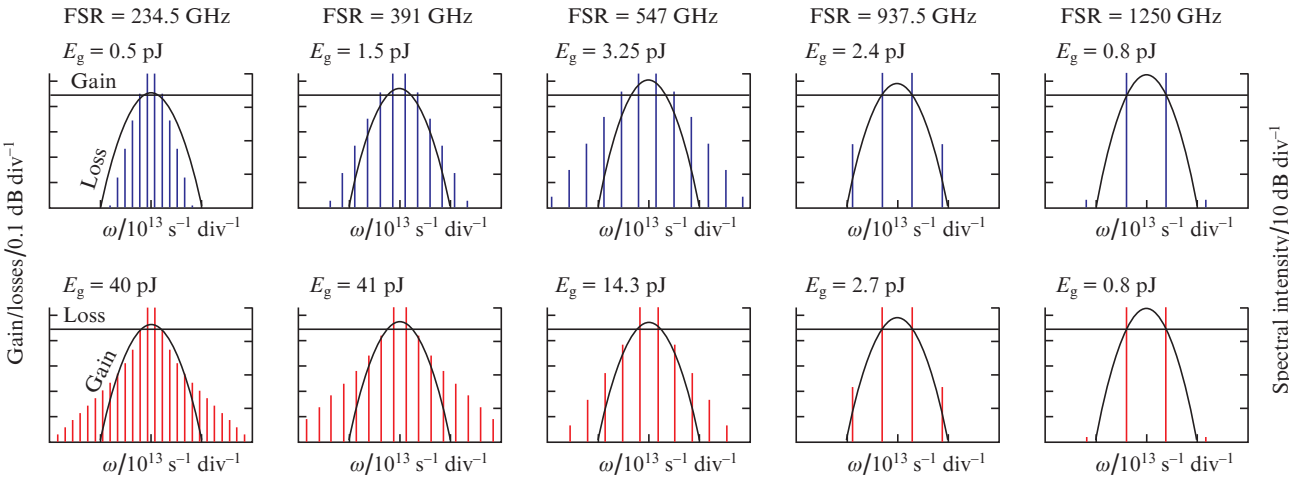

Figure 3. Spectra of the pulse trains obtained as a result of simulation at different FSR repetition rates and the gain saturation energy E_g in the case of anomalous (upper row) and normal (bottom row) cavity dispersion.

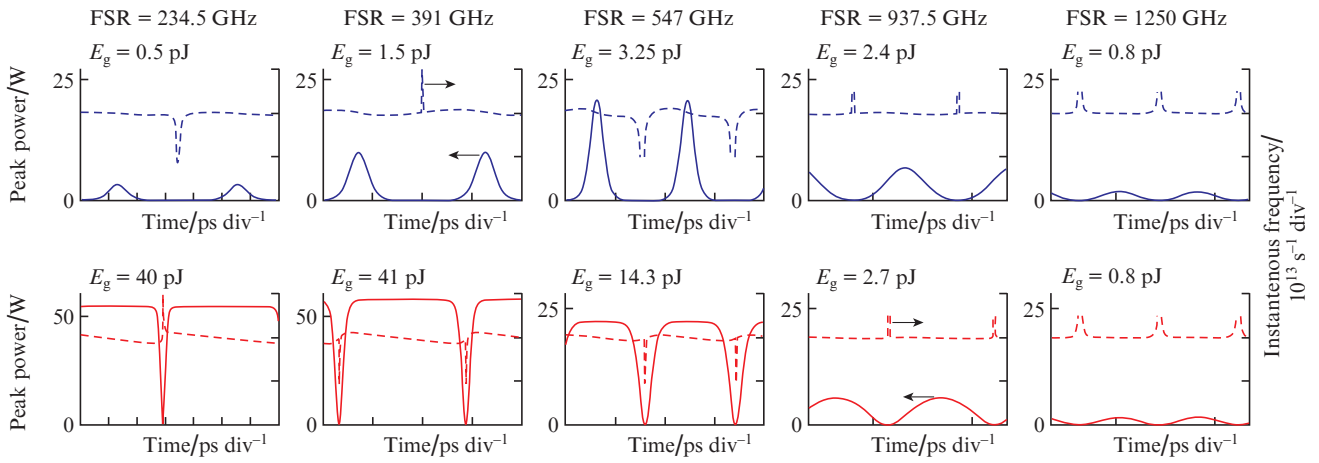

Figure 4. Pulse trains and their instantaneous frequency obtained as a result of simulation at different FSR repetition rates and the gain saturation energy E_g in the case of anomalous (upper row) and normal (lower row) cavity dispersion.

time dependences of successfully generated pulse trains. Even at low saturation energies and low FSR values, not only fundamental but also side modes fall into the region of positive gain. The frequency range, in which it is possible to select the gain in such a way that only two fundamental modes fall into the necessary gain region, begins with FSR ≈ 234.5 GHz; in this case, $E_g \approx 0.5$ pJ. Then, with increasing FSR, the interval of permissible gain values increases (Fig. 5a). At points corresponding to the maximum values of the gain (or the saturation energy E_g), the peak power and width of the pulse spectrum are maximal, whereas the duration is minimal. At sufficiently high peak powers on the graphs of the instantaneous frequency (see Fig. 4), one can see the frequency modulation of the pulses due to the incomplete dispersion compensation of self-phase modulation (SPM). The range of acceptable gain values reaches a maximum when FSR ≈ 700 GHz (Fig. 5a). At higher repetition rates, the gain is limited by the second condition (7), which depends on the selectivity of the intracavity interferometer used. When the gain is close to the threshold, the selectivity of the interferometer used is sufficient to generate a train of pulses with the FSR of more than 1 THz, but the quality of the teain (contrast, peak power, etc.) is significantly reduced, since the intensity of the nonfundamental modes is very small.

We begin the analysis of the results for the normal dispersion of the resonator (Figs 3 and 4, bottom row; Fig. 5b) with high FSR values. At a small (near-threshold) gain and high repetition rates, the situation is virtually indistinguishable from the case of anomalous dispersion – the selectivity of the interferometer ensures the filtration of the fundamental modes, but the gain is sufficient only for the DFWM locking of nonfundamental modes of very low intensity. With a decrease in FSR (i.e., with a decrease in the repetition rate), there appears a principal difference between the two cases. Anomalous dispersion of the resonator compensates for the SPM, which leads to the generation of short soliton-type pulses with a wide spectrum even at low energies and facilitates the generation of nonfundamental modes. The effect of normal dispersion and SPM, on the contrary, is co-directed and promotes the spreading of the pulse. Generation of the nonfundamental modes is weaker in this case, and to increase their intensity it is necessary to increase the pump power. As a result, pulses generated in a resonator with normal dispersion, comparable in spectral width to soliton-type pulses, have a much higher energy and have the form of so-called dark solitons – narrow dips in constant intensity radiation [26, 27]. The range of permissible gain values reaches a maximum at FSR ≈ 300 GHz (Fig. 5b). At lower repetition rates, despite an increase in pulse energy, the magnitude of the maximum gain decreases. This can be explained by the fact that the

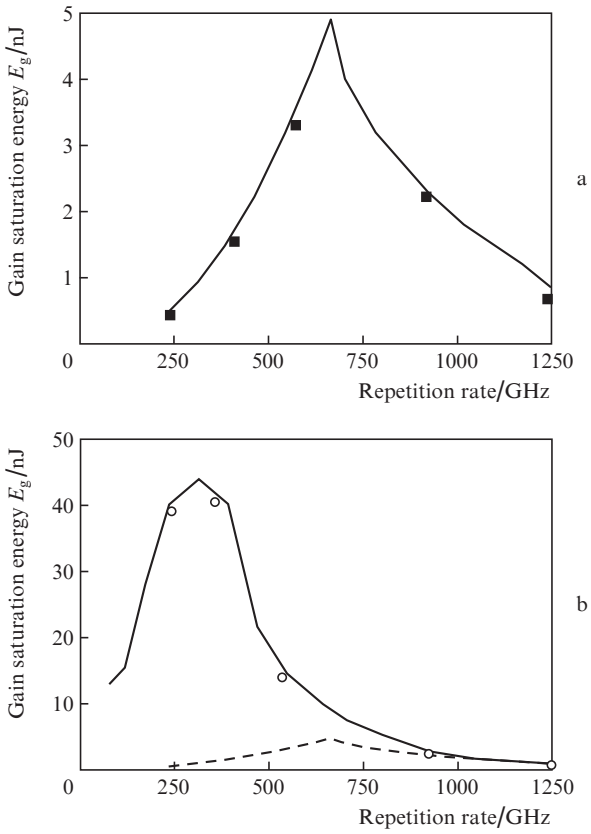

Figure 5. Regions of successful DFWM mode locking in the model under consideration in the case of (a) anomalous and (b) normal dispersion of the resonator. The dashed line corresponds to the curve in Fig. 5a. The symbols show the values of FSR and E_g shown in Figs 3 and 4.

spectral width increases at a given power level due to an increase in duration – the spectrum width of a strongly frequency-modulated pulse is proportional to the duration and chirp (see the leftmost plots of the bottom row in Figs 3 and 4).

At small FSR, the energy of the generated pulses drops sharply. This, as in the case of anomalous dispersion, is caused by the fact that even for small values of G, not only fundamental modes fall into the region of positive gain. Here, however, there is a feature due to the fact that the energy of dark solitons is much higher than the energy of soliton pulses in a resonator with anomalous dispersion, i.e., for generation of pulses in a medium with normal dispersion, even at low repetition frequencies, a sufficiently high pump power level is required. The regions of successful filtering and automatic DFWM mode-locking are compared in Fig. 5b for the case of anomalous and normal dispersion of the resonator.

Note also the dependence of the pulse characteristics on the dispersion $B_{2\Sigma}$ of the resonator. In particular, as the normal dispersion is increased in a certain range of repetition rates, it is possible to substantially increase the energy of the dark soliton. Finding the exact conditions for generation of pulses of maximum energy and increased peak power in this scheme is a separate task that goes beyond the scope of this paper; this problem will be considered elsewhere.

5. Discussion of the results and conclusions

The simulation performed allows us to draw the following conclusions. Mode-locking through DFWM can be realised both with anomalous and normal dispersion of a fibre ring resonator; for its implementation in a real system the intracavity interferometer should have a high selectivity, similar to the selectivity of a high-Q Fabry–Perot interferometer. Generation of pulses with high repetition rates is also facilitated by the presence of a broad gain line of the active medium. When these conditions are met, the laser can generate pulses over a wide range of repetition rates given by the FSR parameter of the interferometer.

For each repetition rate, there is an admissible range of gain values. At a small gain, the characteristics of the pulses generated in the case of anomalous and normal dispersions are close, since the intensity of the nonfundamental modes is very low. With increasing gain, the intensity of the nonfundamental modes increases and the spectrum of the generated pulses is broadened. In the case of anomalous dispersion of the resonator, the generated pulses are soliton-like (the dispersion compensates for self-phase modulation) and short. In this case, an increase in the gain level is limited by a rapid increase in the intensity of the nonfundamental modes, which violates the necessary conditions for the DFWM mode locking. Therefore, for anomalous dispersion of the resonator, the energy of an individual pulse is small and, for practical use, the train of pulses is likely to be further amplified.

On the contrary, normal dispersion of the resonator at a sufficiently high pump level makes it possible to generate pulses of considerable energy (inside the resonator, up to 200 pJ or higher, see Fig. 4, bottom row), and with increasing pump power, the pulse energy can be increased. These pulses have the form of dark solitons with linear frequency modulation. The width of their spectrum is proportional to the product of duration by the amount of chirp. High linearity of the frequency modulation allows a significant compression of the pulse after the chirp compensation at the resonator output. In addition, a sufficiently high peak power of output pulses allows nonlinear pulse compression methods to be used. Thus, lasers with normal dispersion of the resonator and DFWM-based mode locking are extremely promising sources of ultrashort high-repetition-rate pulses. In using a finite pulse compressor based on a length-nonuniform fibre [28–30], the whole system can be made in an all-fibre design.

Acknowledgements. The work was supported by the Russian Science Foundation (Project No. 16-42-02012).

References

1. Haus H.A., Wong W.S. *Rev. Mod. Phys*., **68** (2), 423 (1996).
2. Schibli T.R., Minoshima K., Hong F.-L., Inaba H., Onae A., Matsumoto H., Hartl I., Fermann M.E. *Opt. Lett*., **29**, 2467 (2004).
3. Schliesser A., Picqué N., Hänsch T.W. *Nature Photon.*, **6**, 440 (2012).
4. Habruseva T., O'Donoghue S., Rebrova N., Kéfélian F., Hegarty S.P., Huyet G. *Opt. Lett*., **34**, 3307 (2009).
5. Saarinen E.J., Rantamäki A., Chamorovskiy A., Okhotnikov O.G. *Electron. Lett*., **48**, 1355 (2012).
6. Grudinin A.B., Gray S. *J. Opt. Soc. Am. B*, **14**, 144 (1997).
7. Amrani F., Haboucha A., Salhi M., Leblond H., Komarov A., Grelu Ph., Sanchez F. *Opt. Lett*., **34**, 2120 (2009).
8. Chen C.-J., Wai P.K.A., Menyuk C.R. *Opt. Lett*., **17**, 417 (1992).
9. Lecaplain C., Grelu Ph. *Opt. Express*, **21**, 10897 (2013).
10. Korobko D.A., Okhotnikov O.G., Zolotovskii I.O. *Opt. Lett*., **40** (12), 2862 (2015).
11. Kutz J.N., Collings B.C., Bergman K., Knox W.H. *IEEE J. Quantum Electron*., **34**, 1749 (1998).
12. Korobko D.A., Gumenyuk R., Zolotovskii I.O., Okhotnikov O.G. *Opt. Fiber Technol*., **20** (6), 593 (2014).
13. Zolotovskii I.O., Korobko D.A., Gumenyuk R.V., Ohotnikov O.G. *Quantum Electron*., **45** (1), 26 (2015) [*Kvantovaya Elektron*., **45** (1), 26 (2015)].
14. Andral U., Buguet J., Si Fodil R., Amrani F., Billard F., Hertz E., Grelu Ph. *J. Opt. Soc. Am. B*, **33**, 825 (2016).
15. Franco P., Cristiani I., Midrio M., Romagnoli M., Fontana F. *Opt. Lett*., **20**, 2009 (1995).
16. Yoshida E., Nakazawa M. *Opt. Lett*., **22**, 1409 (1997).
17. Peccianti M., Pasquazi A., Park Y., Moss D.J., Little B.E., Chu S.T., Morandotti R. *Nature Commun*., **3**, 765 (2012).
18. Quiroga-Teixeiro M., Clausen C.B., Sowrensen M.P., Christiansen P.L., Andrekson P.A. *J. Opt. Soc. Am. B*, **15**, 1315 (1998).
19. Sylvestre T., Coen S., Emplit P., Haelterman M. *Opt. Lett*., **27**, 482 (2002).
20. Mao D., Liu X., Sun Z., Lu H., Han D., Wang G., Wang F., *Sci. Rep*., **3**, 3223 (2013).
21. Korobko D.A., Fotiadi A.A., Zolotovskii I.O. *Opt. Express*, **25** (18), 21180 (2017).
22. Andrianov A.V., Mylnikov V.M., Koptev M.Yu., Muravyev S.V., Kim A.V. *Quantum Electron*., **46**, 387 (2016) [*Kvantovaya Elektron*., **46**, 387 (2016)].
23. Fodil R.S., Amrani F., Yang C., Kellou A., Grelu P. *Phys. Rev. A*, **94** (1), 013813 (2016).
24. Agrawal G.P. *Applications of Nonlinear Fiber Optics* (San Diego: Acad. Press, 2001).
25. Luo A.P., Luo Z.C., Xu W.C. *Opt. Lett*., **34** (14), 2135 (2009).
26. Kivshar Y.S., Luther-Davies B. *Phys. Rep.*, **298** (2), 81 (1998).
27. Pitois S., Finot C., Fatome J., Sinardet B., Millot G. *Opt. Commun.*, **260** (1), 301 (2006).
28. Korobko D.A., Okhotnikov O.G., Zolotovskii I.O. *J. Opt. Soc. Am. B*, **30** (9), 2377 (2013).

29. Korobko D.A., Okhotnikov O.G., Stoliarov D.A., Sysoliatin A.A., Zolotovskii I.O. *J. Lightwave Technol.*, **33** (17), 3643 (2015).
30. Zolotovskii I.O., Korobko D.A., Okhotnikov O.G., Stolyarov D.A., Sysolyatin A.A. *Quantum Electron.*, **45**, 844 (2015) [*Kvantovaya Elektron.*, **45**, 844 (2015)].